

# Optimized Data Rate Allocation for Dynamic Sensor Fusion over Resource Constrained Communication Networks

Hyunho Jung<sup>1</sup>, Ali Reza Pedram<sup>1</sup>, Travis Craig Cuvelier<sup>2</sup> and Takashi Tanaka<sup>3</sup>

**Abstract**—This paper presents a new method to solve a dynamic sensor fusion problem. We consider a large number of remote sensors which measure a common Gauss-Markov process and encoders that transmit the measurements to a data fusion center through the resource restricted communication network. The proposed approach heuristically minimizes a weighted sum of communication costs subject to a constraint on the state estimation error at the fusion center. The communication costs are quantified as the expected bitrates from the sensors to the fusion center. We show that the problem as formulated is a difference-of-convex program and apply the convex-concave procedure (CCP) to obtain a heuristic solution. We consider a 1D heat transfer model and 2D target tracking by a drone swarm model for numerical studies. Through these simulations, we observe that our proposed approach has a tendency to assign zero data rate to unnecessary sensors indicating that our approach is sparsity promoting, and an effective sensor selection heuristic.

## I. INTRODUCTION

In this work, we develop techniques to efficiently allocate communication resources in dynamic sensor fusion over a resource-constrained network. Our principle motivation is networked autonomous systems where the communication between sensors and controllers is wireless. Networked autonomous systems play a major role in the heavy industry, transportation, and defense sectors. In such settings, wired communication may be impossible due to physical constraints (such as mobility). Wired communication may also be impractical due to the difficulty of routing and maintaining cables. This latter concern is not without consequence; a report from the US Navy indicates that over 1,000 missions are aborted per year due to wiring faults [1]. Meanwhile, as control systems become more automated and perform more complex tasks, the number of sensor platforms tends to increase. For example, an Airbus A380-1000 model has about 10,000 sensors on its wings alone [2]. In wireless systems, communications resources are inherently constrained. Understanding the impact of control systems on wireless networks, and developing strategies to manage these constrained resources efficiently subject to the particular requirements of control, will help to enable the development of future autonomous systems.

We first give a high-level overview of our contributions before reviewing the literature.

### A. Our contribution

We consider a setup where several remote sensor platforms observe a common Gauss-Markov process and forward these observations to a fusion center over reliable point-to-point binary communication channels. Use of these *uplink* channels incurs a communication cost, quantified as the expected bitrate of a uniquely decodable source code. Given the observations it receives, the fusion center forms an estimate of the state. Using a *downlink* channel, which we assume incurs no cost, the fusion center feeds this estimate back to the sensor platforms. This formulation is applicable to a variety of physical layer resource allocation problems as detailed in (Sections II-A and II-F). Our key contributions are presently summarized:

- We formulate a sensor rate allocation problem. Using entropy-coded dithered predictive quantization (cf. [3], [4]) we show that the expected bitrate required to encode a quantized linear measurement with a specified reconstruction error can be approximated by a particular information measure.
- We propose to minimize a weighted average of these bitrates, over both sensors and a time horizon, subject to a constraint on the error covariance of an linear minimum mean square error estimator at the fusion center. This results in a non-convex optimization.
- We convert the non-convex optimization to difference-of-convex program [5] and optimize via the heuristic convex-concave procedure (CCP). While there is no guarantee that the CCP procedure will produce the global minimum, it is guaranteed to produce a feasible local minimum [5].
- We perform numerical experiments where we apply our approach to a time-invariant heat transfer system and a time-varying drone tracking system. We observed that as the estimator performance constraint is loosened, our algorithm tends to allocate zero data rate to more unneeded sensors. Our proposed approach thus tends to be sparsity-promoting, and may be utilized as a sensor selection heuristic.
- We provide insight into the sparsity promoting aspect of our approach via considering limiting examples in the scalar case.

\*This work is supported by DARPA Grant D19AP00078 and NSF Award 1944318.

<sup>1</sup>Walker Department of Mechanical Engineering, University of Texas at Austin, TX 78712, USA. jung.hyunho@utexas.edu and apedram@utexas.edu

<sup>2</sup>Department of Electrical and Computer Engineering, University of Texas at Austin, TX 78712, USA. tcuvelier@utexas.edu

<sup>3</sup>Department of Aerospace Engineering and Engineering Mechanics, University of Texas at Austin, TX 78712, USA. ttanaka@utexas.edu

## B. Literature review

A portion of this work appears in [6]. In this manuscript, we motivate our problem formulation more concretely with an application to physical layer wireless resource allocation in wireless communications (cf. Section II-F). We also include new, more elucidating simulation results (cf. Section V). Finally, we conclude with an additional discussion of the sparsity-promoting property of our approach (cf. Section VI).

The relevant prior work straddles several research areas, including optimal sensor selection and control with communication constraints, network information theory (in particular, multiterminal rate distortion theory), and resource allocation in wireless communications. We highlight some relevant contributions from these areas, and contrast them with our present work, in the remainder of this section.

1) *Optimal sensor selection and control with communication constraints* : Optimal sensor selection has been a well-studied problem for several decades. Generally speaking, such approaches aim to choose an optimal subset of sensors from given certain number of sensors. Information measures are often incorporated into the objective functions, or the constraints, of the optimization over subsets. Early examples include heuristic subset optimizations that attempted to maximize the trace or determinant of the Fisher information matrix (FIM). For example, [7] proposed a sensor selection method that ranks the participating sensors according to their contribution of location on the large structure. By an iterative technique, the method removes insignificant sensors, resulting in a selected subset of sensors that tend to maximize the trace and determinant of the FIM. [8] performs sensor selection via a genetic algorithm, with the determinant of the FIM as the figure of merit.

More relevant recent results include those that consider Bayesian estimation/tracking. In [9], an entropy-based heuristic for sensor selection is introduced and applied to target localization. A semi-definite programming (SDP) relaxation of a sensor selection problem that minimizes the determinant of the estimation error covariance matrix was proposed in [10]. In [11], the authors use mutual information between the sensors' observation and current target state computed by using particle filter to evaluate the information gain and minimize the expected uncertainty of the target location. In [12], an optimization method is proposed which maximizes Bayesian Fisher Information and mutual information while minimizing the number of selected sensors. The system model in [13] resembles the one in our present work. A fusion center tracks a Gauss-Markov process with incoming observations from multiple remote sensors. A finite horizon optimization problem is proposed to identify a subset of sensors to be transmit their measurements at each time step. The problem is solved heuristically by a re-weighted  $\ell_1$  relaxation. [14] studies sensor selection in aircraft engine health monitoring and performs sensor selection via evaluating entropy.

In this work we do not consider sensor selection, but rather

*sensor rate allocation*. Rather than selecting a subset of sensors, we formulate an optimization problem to minimize a weighted average of data rates from the sensor platforms to the controller. Our present formulation offers additional flexibility; by choosing different weights, one can apply our present formulation to a variety of physical layer resource allocation problems (cf. Section II-F). Notably, we also consider a system model where the sensors have strictly causal feedback access to the fusion center's best estimate. In Section II-A, we argue that this is a reasonable assumption in several interesting and practical regimes.

Some of the prior art on control with communication constraints is also relevant to this work. [15] motivated the use of prefix-free coding and entropy coded dithered quantization (ECDQ) for control subject to data rate constraints. This work was extended to the MIMO case by [4]. In [16], the information-regularized control of a distributed system is studied. The notional objective is reduce inter-subsystem communication while maintaining adequate control cost. The notion of communication cost resembles the one of this work. It was demonstrated that the optimal controller that jointly minimizes the control cost and the required data rate for inter-subsystem communications has a sparse structure. While the communication cost in our present work resembles the one in [16], we consider a significantly different scenario—namely multiagent tracking. Our objective is to minimize bitrate while maintaining a constraint on the estimator mean squared error (MSE).

2) *Multiterminal rate distortion*: In this work, we address a problem that closely resembles the quadratic Gaussian CEO (Chief Executive/Estimation Officer) problem [17]. In the CEO problem, the decoder, corresponding to the “executive” (analogous to the fusion center in this work), receives messages from a set of encoders or “agents”. Each agent observes a measurement of some random state variable that the executive would like to reconstruct. The tradeoff of interest is the sum rate of communication (usually measured in terms of fixed-length coding) versus the distortion in the CEO's estimate. Generally, it is assumed that the agents' measurements are conditionally independent, given the state, and that agents are not allowed to pool their data beforehand. In the “quadratic Gaussian” version of this problem (cf. [18]), agents observe a Gaussian process subject to independent additive Gaussian noise. The distortion metric is (block average) mean squared error. With an eye to distributed tracking, [19] analyzed a causal version of the general CEO problem. A rate-distortion formulation is proposed where Massey's directed information (cf. [20]) is minimized subject to a constraint on the CEO's estimator distortion. This tradeoff is shown to be computable via a convex optimization in the Gaussian case. The rate loss due to the lack of communication between the sensors is also analyzed.

In this work, we deviate from the formulation of the CEO problem in that we minimize a weighted average of the data rates from sensor platforms to the fusion center, rather than just the sum rate. This is advantageous, for example, in an application to physical layer resource allocation (cf.

Section II-F). Most coding schemes for the CEO problem use fixed-length coding. We consider zero-delay uniquely decodable variable length source coding, which may be advantageous in practice. Finally, we consider a setting where the sensors have feedback access to the decoder's estimate. Unfortunately, our lower bounds on codeword length are not completely general (they are with respect to a particular quantization scheme), and we have as-yet been unable to convexify the relevant optimization problem we derive.

3) *Resource allocation for control over wireless networks*: Ultra-low latency reliable wireless communication (ULLRC) has been proposed as an enabler of next-generation networked autonomous systems- in particular for control systems using wireless communication [21] [22]. In the 5G cellular context, ULLRC is characterized by very short end-to-end latencies (on the order of a millisecond) and extremely small error probabilities (on the order of  $10^{-5}$ ) [22]. [23] proposed a prediction-communication co-design approach with a network topology similar to the one considered here. A non-convex optimization was introduced to minimize the bandwidth required to decode a fixed-length message subject to constraints on block error probability and the probabilities of exceeding the latency or prediction error constraints. This approach was shown to effectively improve the tradeoff between reliability and performance (measured in terms of the aforementioned error rate metrics). In this work we consider a different notion of performance, namely estimator MSE. Our scheme is also able to dynamically allocate wireless resources by means of effective source coding; we optimize the actual number of bits conveyed from the sensors to the fusion center. In contrast to [23], we do not include finite-blocklength channel coding in our analysis. In [24], a general feedback control system using ULLRC is abstracted analogously to the CEO problem. The executive is assumed to operate on a fixed schedule and is required to produce its actions by a hard real-time deadline. Different agents make asynchronous linear/Gaussian measurements of a Gauss-Markov dynamical system, and transmit their measurements to the executive over a shared communication channel. The executive's estimator performance is measured in terms of MSE. Polling an observer incurs a communication cost (assumed known a priori), or *airtime*, and a branch and bound approach is applied to schedule the optimal sequence of observers that can be polled before the deadline. Our present work could be seen as optimizing the total (expected) airtime required to achieve some estimator performance (cf. Sec. II-F).

The recent survey, [25], on control systems incorporating wireless communication contains many relevant references, several practical case studies, and a detailed overview of a framework for control/communication co-design. It is argued that wireless systems for control applications should be dependable (measured in terms of control performance and stability), adaptive (reconfigurable), and efficient (with respect to the use of resources like time, bandwidth, and power). A control-guided communication approach where messages are transmitted according to a self-triggered pro-

tol. This approach was shown to be effective through experiments in a cyber-physical testbed. In this work, we consider synchronous communication, which may be a necessity for control over congested networks. Our sensor rate allocation scheme is also inherently dynamic; in simulation, we demonstrate that different subsets of sensors are assigned nonzero bitrates over time. Furthermore, our choice to minimize bitrate allows us to draw direct link between the utilization of physical layer resources and estimator performance, improving efficiency (at least on average).

### C. Organization and notation

This paper is organized as follows. Section II reviews ECDQ, defines the notion of communication cost, and connects this cost to the mutual information (MI) between two Gaussian random variables that arise in Kalman filtering. The sensor rate allocation (SRA) problem is proposed. We conclude the section with an application example motivated by physical layer resource allocation in a remote sensing scenario. In Section III, we show that the communication cost can be written in terms of error covariance matrices from Kalman filtering. In these terms, we convert the SRA optimization to a difference-of-convex program. Section IV defines an iterative heuristic algorithm based on the convex-concave procedure (CCP) to attack the resulting non-convex optimization. Our numerical studies are introduced in Section V. We provide insight into the sparsity-promoting nature of our approach in Section VI. We conclude in Section VII.

Lower case boldface symbols such as  $\mathbf{x}$  denotes random variables and  $\mathbf{x}_{1:t} = (\mathbf{x}_1, \dots, \mathbf{x}_t)$  denotes the random process. We take up on standard information-theoretic notation from [26]: the entropy of a discrete random variable  $\mathbf{x}$  is denoted by  $H(\mathbf{x})$ , while the differential entropy of a continuous random variable  $\mathbf{x}$  is denoted by  $h(\mathbf{x})$ . The mutual information between  $\mathbf{x}$  and  $\mathbf{y}$  is denoted by  $I(\mathbf{x}; \mathbf{y})$ , and the relative entropy is denoted by  $D(\cdot \| \cdot)$ .  $\mathbb{S}^n$  represents the set of symmetric matrices of size  $n \times n$ .  $X \in \mathbb{S}^n$ ,  $X \in \mathbb{S}_+^n$  or  $X \succeq 0$  indicates that  $X$  is a positive semi-definite matrix, and  $X \in \mathbb{S}_{++}^n$  or  $X \succ 0$  represents that  $X$  is a positive definite matrix. We denote the set of natural numbers  $1, 2, \dots, M$  as  $1 : M$ , and the set of positive natural numbers as  $\mathbb{N}^+$ .

## II. PROBLEM FORMULATION

We consider discrete-time estimation of a Gauss-Markov source and assume the source is an  $n$ -dimensional random process defined via

$$\mathbf{x}_{t+1} = A\mathbf{x}_t + F\mathbf{w}_t, \quad \mathbf{w}_t \stackrel{i.i.d.}{\sim} \mathcal{N}(0, I), \quad t = 1, 2, \dots, T \quad (1)$$

with initial condition  $\mathbf{x}_1 \sim \mathcal{N}(0, P_{1|1})$ , where  $P_{1|1} \in \mathbb{S}_+^n$  and  $A \in \mathbb{R}^{n \times n}$ . We consider remote estimation over a star-like sensor network, as shown in Fig 1. Each of the  $M$  sensors makes a noiseless, scalar, linear measurement of the state vector. At time  $t$ , sensor  $i$  observes  $\mathbf{y}_{i,t} = C_i \mathbf{x}_t$  for some  $C_i \in \mathbb{C}^{1 \times n}$ . Concatenating the measurements from each sensor into  $\mathbf{y}_t \in \mathbb{C}^M$ , we have

$$\mathbf{y}_t = C\mathbf{x}_t \quad (2a)$$

where

$$\mathbf{y}_t = \begin{bmatrix} y_{1,t} \\ \vdots \\ y_{M,t} \end{bmatrix}, \quad C = \begin{bmatrix} C_1 \\ \vdots \\ C_M \end{bmatrix}. \quad (2b)$$

We assume that sensors must convey these measurements to the fusion center over a resource-constrained communication network, as detailed in the sequel. Throughout the paper, we assume that the pair (A,C) is observable.

#### A. Data fusion over resource-constrained network

We assume the platforms operate synchronously in discrete-time, analogous to a CAN-bus-like system. At time  $t$ , we assume that sensor  $i$  encodes  $y_{i,t}$  into a binary codeword, say  $\mathbf{z}_{i,t}$ , from a uniquely decodable variable-length code. The length of the codeword  $\mathbf{z}_{i,t}$ , in bits, is denoted  $\ell_{i,t}$ . The expected length of  $\ell_{i,t}$  measures the bitrate of uplink communication from the  $i^{\text{th}}$  sensor platform to the fusion center, and provides a notion of communication cost. In the CAN protocol, a packet frame consists of a header and a trailer in addition to the data field. For the sake of simplicity, we neglect the contributions from these components to the network's bitrates. We assume that the uplink communication is *reliable* in the sense that the packet  $\mathbf{z}_{i,t}$  is received without error before time  $t+1$ .

Having received packets from each of the  $M$  platforms, the fusion center decodes packets and computes the linear minimum mean-square error (LMMSE) estimate  $\hat{\mathbf{x}}_{t|t}$ . The fusion center also calculates a step-ahead prediction  $\hat{\mathbf{x}}_{t+1|t}$  based on least mean-square-error estimate  $\hat{\mathbf{x}}_{t|t}$  and the source process (1). Once the prediction  $\hat{\mathbf{x}}_{t+1|t}$  is calculated, the fusion center transmits the prediction back to all the sensors as shown in Fig. 1. Access to  $\hat{\mathbf{x}}_{t+1|t}$  at the sensor platforms allow them to apply *predictive quantization* at time step  $t+1$ . Quantization and encoding the *innovation*  $y_{i,t+1} - C_i \hat{\mathbf{x}}_{t+1|t}$ , rather than  $y_{i,t+1}$  directly, helps to reduce the expected codeword length (cf. [27] and [4]).

We neglect the communication cost associated with the downlink communication and assume that the sensors receive  $\hat{\mathbf{x}}_{t+1|t}$  exactly. These assumptions are appropriate in a variety of circumstances. The fusion center's downlink message could encode a finely quantized version of  $\hat{\mathbf{x}}_{t+1|t}$ . If the fusion center is not energy constrained, using high power it can transmit this message reliably to all of the  $M$  sensor platforms. This notion would also be useful in scenarios where each individual platform can decode the messages from the other platforms directed towards the fusion center. This is possible, generally speaking, when the channel capacities between platforms exceeds the capacity between any one platform and the fusion center. This occurs, for example, in a line-of-sight communication setting where the distance between the individual sensor platforms is small compared with the distance between the platforms and the fusion center.

#### B. Entropy-coded dithered quantization

We assume that sensor platforms discretize, and encode their measurements into binary codewords, using *entropy-coded dithered quantization* (ECDQ) [28]. Define a uniform

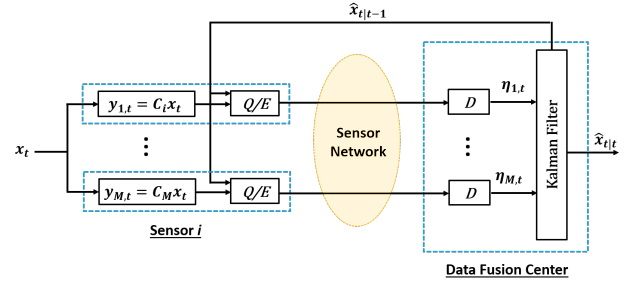


Fig. 1. Data fusion center and distributed sensors. “Q/E” represents the quantizer/encoder module whereas “D” represents the decoder module.

scalar quantizer with sensitivity  $\Delta$  via

$$Q_{\Delta}(z) = k\Delta \text{ if } (k - \frac{1}{2})\Delta \leq z < (k + \frac{1}{2})\Delta. \quad (3)$$

Essentially, the function  $Q_{\Delta}$  rounds its input to the nearest multiple of  $\Delta$ . *Dithering* introduces intentional randomness into the quantization process to make the quantization error tractable. Let  $\mathbf{z}$  be a random variable that we like to encode, and let  $\xi \sim \text{unif}[-\frac{\Delta}{2}, \frac{\Delta}{2}]$  independent of  $\mathbf{z}$ . Define the *quantization*

$$\mathbf{q} = Q_{\Delta}(\mathbf{z} + \xi). \quad (4)$$

In general,  $\mathbf{q}$  is a discrete random variable with countable support. Define the *reconstruction*

$$\boldsymbol{\eta} = \mathbf{q} - \xi. \quad (5)$$

It can be shown (cf. [3], [4]) that

$$\boldsymbol{\eta} = \mathbf{z} + \mathbf{v} \quad (6)$$

where  $\mathbf{v} \sim \text{unif}[-\frac{\Delta}{2}, \frac{\Delta}{2}]$  and independent of  $\mathbf{z}$ . Note that the *same* realization of the dither signal  $\xi$  is used in the quantization and reconstruction steps.

Fig. 2 illustrates the use of dithering in our communication network model. We assume that each sensor platform shares a common dither signal with fusion center. At time  $t$ , denote the  $i^{\text{th}}$  platform's dither signal  $\xi_{i,t}$ . The stochastic process (defined over time and platforms)  $\{\xi_{i,t}\}_{i \in 1:M, t \in \mathbb{N}^+}$  consists of mutually independent uniform random variables

$$\xi_{i,t} \sim \text{unif}[-\frac{\Delta_{i,t}}{2}, \frac{\Delta_{i,t}}{2}] \quad (7)$$

where the sensitivities  $\Delta_{i,t}$  will be designed in the sequel. The dither process is also independent of  $\{\mathbf{x}_t\}_{t \in \mathbb{N}^+}$ . At time  $t$ , platform  $i$  computes the Kalman innovation corresponding to its measurement via

$$\boldsymbol{\theta}_{i,t} = \mathbf{y}_{i,t} - C_i \hat{\mathbf{x}}_{t|t-1}. \quad (8)$$

It then computes the dithered quantization

$$\mathbf{q}_{i,t} = Q_{\Delta_{i,t}}(\boldsymbol{\theta}_{i,t} + \xi_{i,t}).$$

The sensor platform uses *lossless* variable-length *entropy coding* to encode  $\mathbf{q}_{i,t}$  into a finite-length binary string. Denote this *codeword*  $\mathbf{z}_{i,t}$ . The length of  $\mathbf{z}_{i,t}$  is a random variable, denote  $\ell_{i,t}$ . It can be shown that there exists a

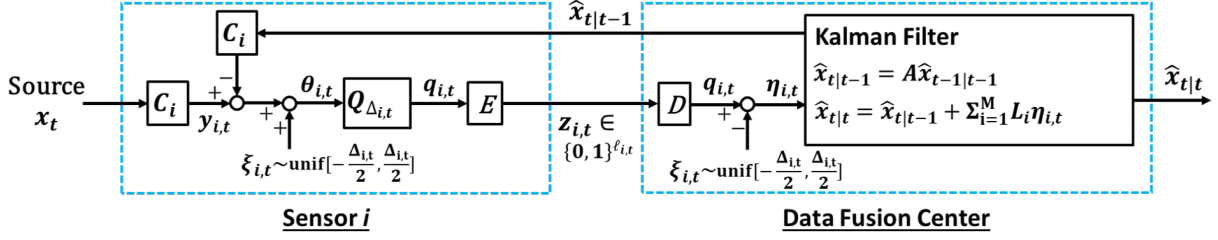


Fig. 2. This figure gives an overview of the communication architecture between an individual sensor platform and the fusion center. Note that the dither signal,  $\xi_{i,t}$  is assumed to be known at both the sensor platform and the fusion center. In practice, this “shared randomness” can be accomplished by using synchronized pseudorandom number generators between each sensor platform and the fusion center.

lossless source code, adapted to the conditional probability mass function of  $\mathbf{q}_{i,t}$  given  $\xi_{i,t}$ , with expected codeword length satisfying (cf. [26], Theorem 5.5.1 and Exercise 5.28))

$$H(\mathbf{q}_{i,t}|\xi_{i,t}) \leq \mathbb{E}(\ell_{i,t}) < H(\mathbf{q}_{i,t}|\xi_{i,t}) + 1. \quad (9)$$

Alternative, more tractable bounds on codeword length are developed in the next section. Since the binary communication channel from the sensor platform to the fusion center is assumed to be noiseless the sensor platform receives  $\mathbf{z}_{i,t}$  exactly. Since the entropy code is lossless, the decoder at the fusion center recovers  $\mathbf{q}_{i,t}$  exactly. The decoder then computes the dithered reconstruction

$$\boldsymbol{\eta}_{i,t} = \mathbf{q}_{i,t} - \xi_{i,t}. \quad (10)$$

Using (4,5,6) we have

$$\boldsymbol{\eta}_{i,t} = \boldsymbol{\theta}_{i,t} + \mathbf{v}_{i,t}, \text{ where } \mathbf{v}_{i,t} \sim \text{unif}\left[-\frac{\Delta_{i,t}}{2}, \frac{\Delta_{i,t}}{2}\right]. \quad (11)$$

It can be shown that the random variables  $\{\mathbf{v}_{i,t}\}_{i \in 1:M, t \in \mathbb{N}^+}$  are mutually independent and independent of  $\{\boldsymbol{\theta}_{i,t}\}_{i \in 1:M, t \in \mathbb{N}^+}$  [4] [3]. An end-to-end model of entropy coded dithered quantization is shown in Fig 3. The joint distributions of the random variables in Fig 3 are identical to those in Fig 2.

### C. Communication cost approximation

We define the communication cost associated with the  $i^{\text{th}}$  sensor over some time horizon  $T$  as the time-averaged expected codeword length, e.g.

$$R_i = \frac{1}{T} \sum_{t=1}^T \mathbb{E}(\ell_{i,t}). \quad (12)$$

Under several reasonable architectures from wireless communications, this cost is an effective surrogate for the (expected) amount of physical layer resources consumed by the  $i^{\text{th}}$  platform on the uplink (cf. Section II-F). Equation (9) gave a bound on  $\mathbb{E}(\ell_{i,t})$  in terms of a conditional entropy. In the following lemma, we express these bounds in terms of a mutual information.

**Lemma 1:** For every sensor  $i$  and time step  $t$ , the expected codeword length satisfies

$$I(\boldsymbol{\theta}_{i,t}; \boldsymbol{\eta}_{i,t}) \leq \mathbb{E}(\ell_{i,t}) < I(\boldsymbol{\theta}_{i,t}; \boldsymbol{\eta}_{i,t}) + 1$$

where the mutual information is taken with respect to the joint distribution of  $\boldsymbol{\theta}_{i,t}$  and  $\boldsymbol{\eta}_{i,t}$  induced by the model in Fig. 3.

*Proof:* Recall that  $\boldsymbol{\eta}_{i,t} = \mathbf{q}_{i,t} - \xi_{i,t}$ . Thus

$$H(\mathbf{q}_{i,t}|\xi_{i,t}) = H(\boldsymbol{\eta}_{i,t}|\xi_{i,t}) \quad (13)$$

Thus, by (9), we have

$$H(\boldsymbol{\eta}_{i,t}|\xi_{i,t}) \leq \mathbb{E}(\ell_{i,t}) < H(\boldsymbol{\eta}_{i,t}|\xi_{i,t}) + 1. \quad (14)$$

Under the joint distribution of  $\boldsymbol{\theta}_{i,t}$  and  $\boldsymbol{\eta}_{i,t}$  induced by the model in Fig. 2 it can be shown that (cf. [3], [4], Lemma 1))

$$H(\boldsymbol{\eta}_{i,t}|\xi_{i,t}) = I(\boldsymbol{\theta}_{i,t}; \boldsymbol{\eta}_{i,t}). \quad (15)$$

The results of the previous section show that the joint distribution of  $\boldsymbol{\theta}_{i,t}$  and  $\boldsymbol{\eta}_{i,t}$  induced by the model in Fig. 3 is equivalent to the joint distribution induced by Fig. 2. Substituting (15) into (14) completes the proof. ■

Note that  $\boldsymbol{\theta}_{i,t}$  and  $\boldsymbol{\eta}_{i,t}$  are non-Gaussian. Directly evaluating the mutual information  $I(\boldsymbol{\theta}_{i,t}; \boldsymbol{\eta}_{i,t})$  is rather difficult. In [29], an approach to evaluating this mutual information was proposed via defining an “jointly Gaussian” version of the architecture in Fig. 3, shown here in Fig. 4. Define

$$V_{i,t} = \frac{\Delta_{i,t}^2}{12}. \quad (16)$$

Essentially, the uniform quantization noise  $\mathbf{v}_{i,t}$  in Fig. 3 is replaced with additive Gaussian noise, independent over sensors and time, with the same mean and covariances, i.e.

$$\mathbf{v}_{i,t}^G \sim \mathcal{N}(0, V_{i,t}), \text{ independent over } t, i, \text{ and independent of } \{\mathbf{x}_t\}_{t \in \mathbb{N}^+}. \quad (17)$$

Under this model, the measurements and reconstructions are jointly Gaussian, and denoted  $\boldsymbol{\theta}_{i,t}^G$  and  $\boldsymbol{\eta}_{i,t}^G$  respectively. Assume that the dynamical systems in Fig. 3 and Fig. 4 have initial conditions with identical first and second moments. It follows from the linearity of the models in Fig. 3 and Fig. 4, and in particular the fact that the Kalman filter recursions are identical, that the stochastic processes  $\{\mathbf{x}_{t|t}^G, \mathbf{x}_{t|t-1}^G, \boldsymbol{\theta}_t^G, \boldsymbol{\eta}_t^G\}_{t=1,2,\dots,T}$  and  $\{\mathbf{x}_{t|t}, \mathbf{x}_{t|t-1}, \boldsymbol{\theta}_t, \boldsymbol{\eta}_t\}_{t=1,2,\dots,T}$  have identical first and second moments.

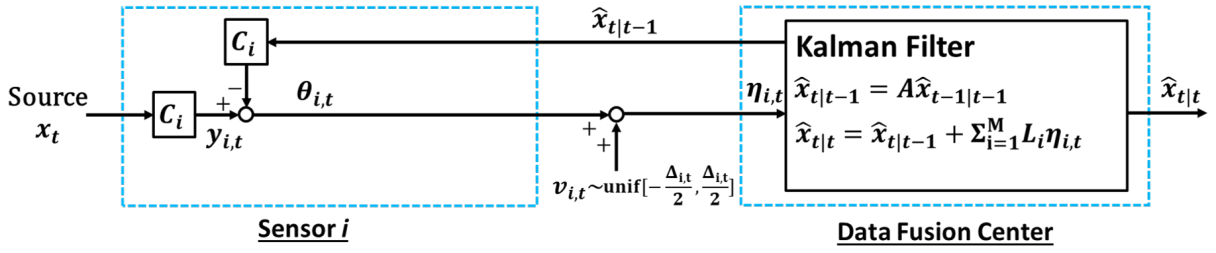


Fig. 3. The net effect of the ECDQ scheme is that, from the each sensor platform, the fusion center receives a linear measurement corresponding to the platform's Kalman innovation corrupted by additive *uniform* noise.

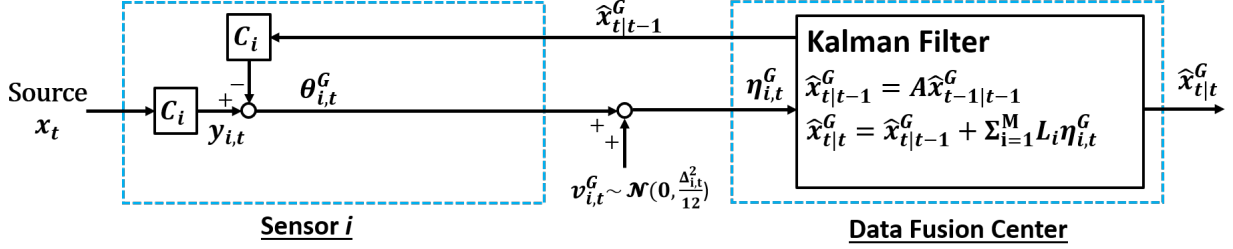


Fig. 4. A "jointly Gaussian" version of the architecture shown in Fig. 3. The uniform noise in Fig. 3 is replaced with Gaussian noise with the same first and second order statistics. The process defined by the random variables in this figure is jointly Gaussian and has identical first and second moments to the process defined by the random variables in Fig. 3.

The next lemma shows that  $I(\theta_{i,t}; \eta_{i,t})$  can be bounded to within two bits of  $I(\theta_{i,t}^G; \eta_{i,t}^G)$ .

**Lemma 2:**

$$I(\theta_{i,t}^G; \eta_{i,t}^G) \leq I(\theta_{i,t}; \eta_{i,t}) < I(\theta_{i,t}^G; \eta_{i,t}^G) + \frac{1}{2} \log \frac{2\pi e}{12}.$$

*Proof:* The lower bound follows from [29, Lemma C.1].

To see the upper bound, first expand the mutual information in terms of differential entropy

$$I(\theta_{i,t}; \eta_{i,t}) = h(\theta_{i,t}) - h(\theta_{i,t} | \eta_{i,t}) \quad (18)$$

$$= h(\theta_{i,t}) - h(\eta_{i,t} - \mathbf{v}_{i,t} | \eta_{i,t}) \quad (19)$$

$$= h(\theta_{i,t}) - h(\mathbf{v}_{i,t}), \quad (20)$$

where (19) follows from the definition of  $\theta_{i,t}$  and (20) follows since  $\mathbf{v}_{i,t}$  and  $\eta_{i,t}$  are independent (cf. below (11)). Likewise

$$I(\theta_{i,t}^G; \eta_{i,t}^G) = h(\theta_{i,t}^G) - h(\mathbf{v}_{i,t}^G) \quad (21)$$

Gaussian random variables have the maximum entropy among all random variables with the same variance (cf. [26, Theorem 8.6.5]). Thus, we have

$$h(\theta_{i,t}) \leq h(\theta_{i,t}^G). \quad (22)$$

Furthermore, by applying the definition of differential entropy, expanding the PDF of  $\mathbf{v}_{i,t}^G$ , and recalling that  $\mathbf{v}_{i,t}^G$  and  $\mathbf{v}_{i,t}$  have the same variance, we have

$$h(\mathbf{v}_{i,t}) = h(\mathbf{v}_{i,t}^G) - D(\mathbf{v}_{i,t} || \mathbf{v}_{i,t}^G) \quad (23)$$

$$= h(\mathbf{v}_{i,t}^G) - \frac{1}{2} \log \frac{2\pi e}{12}. \quad (24)$$

Thus, recalling both (21) and (18), and subtracting both sides of (23) from the respective sides of (22) gives

$$\begin{aligned} I(\theta_{i,t}; \eta_{i,t}) &\leq h(\theta_{i,t}^G) - h(\mathbf{v}_{i,t}^G) + \frac{1}{2} \log \frac{2\pi e}{12} \\ &= I(\theta_{i,t}^G; \eta_{i,t}^G) + \frac{1}{2} \log \frac{2\pi e}{12}. \end{aligned}$$

■

Using Lemma 2, we can generate a new bound from Lemma 1 via

$$I(\theta_{i,t}^G; \eta_{i,t}^G) \leq \mathbb{E}(\ell_{i,t}) < I(\theta_{i,t}^G; \eta_{i,t}^G) + \underbrace{1 + \frac{1}{2} \log \frac{2\pi e}{12}}_{\approx 1.254 \text{ [bits]}}. \quad (25)$$

We will use the expression for  $I(\theta_{i,t}^G; \eta_{i,t}^G)$  to approximate the communication cost in (12). In particular we define  $R_i^a$  as the *approximate* time-averaged expected bitrate for the  $i^{\text{th}}$  sensor via

$$R_i^a = \frac{1}{T} \sum_{t=1}^T I(\theta_{i,t}^G; \eta_{i,t}^G) \quad (26)$$

Since  $\mathbf{v}_{i,t}^G \sim \mathcal{N}(0, \Delta_{i,t}^2/12)$ , the mutual information  $I(\theta_{i,t}^G; \eta_{i,t}^G)$  is a function of the quantizer sensitivity  $\Delta_{i,t}$ . Tuning the set of sensitivities allows us to adjust the data rates allocated to different sensors over time. We demonstrate this explicitly in Section III. In the remainder of this section, we will use some properties from Kalman filters to extend our notion of "second order equivalence" between the random variables in Fig. 3 and Fig. 4 to the case of multiple sensors. We write  $I(\theta_{i,t}^G; \eta_{i,t}^G)$  in terms of another mutual information, and define the sensor rate allocation problem.

#### D. Linear minimum mean square error estimation

We consider sensor fusion in the setting that where the fusion center's observations follow the models of either Fig. 2 or Fig. 4. In both cases, the fusion center uses a Kalman filter to recursively estimate  $\mathbf{x}_t$ . When all sensors conform to the non-Gaussian model of Fig. 2, at time  $t$ , the Kalman filter computes

$$\hat{\mathbf{x}}_{t|t-1} = \text{LMMSE estimate of } \mathbf{x}_t \text{ given } \{\boldsymbol{\eta}_{i,k}\}_{i \in 1:M, k \in 1:t-1} \quad (27a)$$

and

$$\hat{\mathbf{x}}_{t|t} = \text{LMMSE estimate of } \mathbf{x}_t \text{ given } \{\boldsymbol{\eta}_{i,k}\}_{i \in 1:M, k \in 1:t}. \quad (27b)$$

Conversely, in the case where all sensors conform to the Gaussian model (cf. Fig. 4), the LMMSE estimate computed by the Kalman filter corresponds to the minimum mean square error (MMSE) estimate, e.g.

$$\hat{\mathbf{x}}_{t|t-1}^G = \mathbb{E}(\mathbf{x}_t | \boldsymbol{\eta}_{1:t-1}^G) \quad (28a)$$

and

$$\hat{\mathbf{x}}_{t|t}^G = \mathbb{E}(\mathbf{x}_t | \boldsymbol{\eta}_{1:t}^G). \quad (28b)$$

Analogously to the previous section, if the initial conditions in both the Gaussian and non-Gaussian systems have identical mean and covariance matrices, the Kalman filter recursions, in particular the achieved mean squared errors, are identical. Thus, for any fixed choice of quantizer sensitivities  $\Delta_{i,t}$  the estimator in Fig. 2 (equivalently, Fig. 3) achieves the same MSE performance as the estimator in Fig. 4. We now use some properties of MMSE estimation in the Gaussian case to simplify the mutual information  $I(\boldsymbol{\theta}_{i,t}^G; \boldsymbol{\eta}_{i,t}^G)$ .

Let  $V_t$  be a diagonal matrix such that  $V_{i,t}$  is the  $i$ th diagonal entry, e.g.

$$V_t = \begin{bmatrix} \frac{\Delta_{1,t}^2}{12} & 0 & \dots & 0 \\ 0 & \frac{\Delta_{2,t}^2}{12} & \dots & 0 \\ \vdots & \vdots & \ddots & \vdots \\ 0 & 0 & \dots & \frac{\Delta_{M,t}^2}{12} \end{bmatrix} \quad (29)$$

The Kalman gain at time  $t$  is given by the forward Riccati recursion via

$$L_t = P_{t|t-1} C^\top (C P_{t|t-1} C^\top + V_t)^{-1}. \quad (30)$$

Define  $P_{t|t} \in \mathbb{S}_{++}^n$  and  $P_{t+1|t} \in \mathbb{S}_{++}^n$  as the estimation error covariances  $P_{t|t} = \text{Cov}(\mathbf{x}_t - \hat{\mathbf{x}}_{t|t}^G)$  and  $P_{t+1|t} = \text{Cov}(\mathbf{x}_{t+1} - \hat{\mathbf{x}}_{t+1|t}^G)$ . These matrices satisfy the recursion

$$P_{t|t}^{-1} = P_{t|t-1}^{-1} + C^\top V_t^{-1} C \quad (31a)$$

$$P_{t+1|t} = A P_{t|t} A^\top + F F^\top. \quad (31b)$$

We reiterate that due to the ‘‘second order equivalence’’ between the Gaussian and non-Gaussian systems, we have for all  $t$

$$P_{t|t} = \text{Cov}(\mathbf{x}_t - \hat{\mathbf{x}}_{t|t}) \quad (32)$$

and

$$P_{t+1|t} = \text{Cov}(\mathbf{x}_{t+1} - \hat{\mathbf{x}}_{t+1|t}). \quad (33)$$

The following technical lemma, proved using ideas from Kalman filtering in the Gaussian case, will prove useful in the subsequent sections.

**Lemma 3:** If  $L_t$  is given by (30), then  $I(\boldsymbol{\theta}_{i,t}^G; \boldsymbol{\eta}_{i,t}^G) = I(\mathbf{x}_t; \boldsymbol{\eta}_{i,t}^G | \boldsymbol{\eta}_{1:t-1}^G)$ .

*Proof:* Equality of Lemma 3 can be divided into two inequality conditions as

$$I(\boldsymbol{\theta}_{i,t}^G; \boldsymbol{\eta}_{i,t}^G) \leq I(\mathbf{x}_t; \boldsymbol{\eta}_{i,t}^G | \boldsymbol{\eta}_{1:t-1}^G) \quad (34a)$$

$$I(\boldsymbol{\theta}_{i,t}^G; \boldsymbol{\eta}_{i,t}^G) \geq I(\mathbf{x}_t; \boldsymbol{\eta}_{i,t}^G | \boldsymbol{\eta}_{1:t-1}^G). \quad (34b)$$

Recall that if that random variables  $(\mathbf{x}, \mathbf{y})$  are independent of  $\mathbf{z}$ , then  $I(\mathbf{x}; \mathbf{y} | \mathbf{z}) = I(\mathbf{x}; \mathbf{y})$ . The first inequality is shown via

$$I(\mathbf{x}_t; \boldsymbol{\eta}_{i,t}^G | \boldsymbol{\eta}_{1:t-1}^G) = I(\mathbf{x}_t - \hat{\mathbf{x}}_{t|t-1}^G; C_i(\mathbf{x}_t - \hat{\mathbf{x}}_{t|t-1}^G) + \mathbf{v}_{i,t}^G | \boldsymbol{\eta}_{1:t-1}^G) \quad (35a)$$

$$= I(\mathbf{x}_t - \hat{\mathbf{x}}_{t|t-1}^G; C_i(\mathbf{x}_t - \hat{\mathbf{x}}_{t|t-1}^G) + \mathbf{v}_{i,t}^G) \quad (35b)$$

$$= I(\mathbf{x}_t - \hat{\mathbf{x}}_{t|t-1}^G; \boldsymbol{\eta}_{i,t}^G) \geq I(C_i(\mathbf{x}_t - \hat{\mathbf{x}}_{t|t-1}^G); \boldsymbol{\eta}_{i,t}^G) \quad (35c)$$

$$= I(\boldsymbol{\theta}_{i,t}^G; \boldsymbol{\eta}_{i,t}^G).$$

The first equality, (35a) follows since  $\hat{\mathbf{x}}_{t|t-1}^G$  is a deterministic (in fact, linear) function of  $\boldsymbol{\eta}_{1:t-1}^G$ . In the Gaussian case, the measurement error  $\mathbf{x}_t - \hat{\mathbf{x}}_{t|t-1}^G$  and measurement noise  $\mathbf{v}_{i,t}^G$  are independent of the prior measurements, leading to (35b). The former follows from the orthogonality principle. Finally, (35c) follows from the data processing inequality in [26].

To show the second inequality condition  $I(\boldsymbol{\theta}_{i,t}^G; \boldsymbol{\eta}_{i,t}^G) \geq I(\mathbf{x}_t; \boldsymbol{\eta}_{i,t}^G | \boldsymbol{\eta}_{1:t-1}^G)$ , first expand  $I(\boldsymbol{\theta}_{i,t}^G; \boldsymbol{\eta}_{i,t}^G)$  via

$$I(\boldsymbol{\theta}_{i,t}^G; \boldsymbol{\eta}_{i,t}^G) = I(C_i(\mathbf{x}_t - \hat{\mathbf{x}}_{t|t-1}^G); C_i(\mathbf{x}_t - \hat{\mathbf{x}}_{t|t-1}^G) + \mathbf{v}_{i,t}^G) = I(C_i(\mathbf{x}_t - \hat{\mathbf{x}}_{t|t-1}^G); C_i(\mathbf{x}_t - \hat{\mathbf{x}}_{t|t-1}^G) + \mathbf{v}_{i,t}^G | \boldsymbol{\eta}_{1:t-1}^G) \quad (36a)$$

$$= I(\mathbf{y}_{i,t}; \boldsymbol{\eta}_{i,t}^G | \boldsymbol{\eta}_{1:t-1}^G) \quad (36b)$$

$$\geq I(\mathbf{x}_t; \boldsymbol{\eta}_{i,t}^G | \boldsymbol{\eta}_{1:t-1}^G). \quad (36c)$$

As in (35b), (36a) follows since the measurement error and additive noise is independent of past measurements. Since  $\hat{\mathbf{x}}_{t|t-1}^G$  is a deterministic function of  $\boldsymbol{\eta}_{1:t-1}^G$  (36b) then follows. Finally, (36c) follows from the data processing inequality, from the since  $\mathbf{x}_t \leftrightarrow \mathbf{y}_{i,t} \leftrightarrow \boldsymbol{\eta}_{i,t}^G$  forms a Markov chain given  $\boldsymbol{\eta}_{1:t-1}^G$ . In other words,  $\mathbf{x}_t$  and  $\boldsymbol{\eta}_{i,t}^G$  are conditionally independent given  $\mathbf{y}_{i,t}$  and  $\boldsymbol{\eta}_{1:t-1}^G$ . ■

#### E. The Sensor Rate Allocation (SRA) Problem

We now propose the optimization problem to be studied in the remainder of this paper. We propose to minimize a weighted average of the approximate data rates  $R_i^a$  assigned to each sensor  $i = 1, 2, \dots, M$  subject to a constraint on the MSE performance of the fusion center's estimator. Define a

set of positive weights  $\alpha_i$ ,  $i \in 1 : M$  to represent the cost of transmitting a single bit from platform  $i$  to the fusion center. The total communication cost is  $\sum_{i=1}^M \alpha_i R_i$ , where  $R_i$  is defined in (12). The approximate cost, defined in terms of the approximate bitrates (cf. (26)), is defined as  $\sum_{i=1}^M \alpha_i R_i^a$ . Our decision variables are the sensor platforms' quantizer sensitivities, e.g.  $\{\Delta_{i,t}\}_{i \in 1:M, t \in 1:T}$ . Via (29), it can be seen that for any time  $t$  the set of feasible quantizer sensitivities are in one-to-one correspondence with the set of diagonal, PSD matrices. Let the set of positive semi-definite diagonal  $M \times M$  matrices be denoted  $\mathbb{D}_+^M$ . For  $\beta$  the constraint on the fusion center's MSE, we define the sensor rate allocation problem as

$$\min_{\substack{V_i \in \mathbb{D}_+^M \\ t \in 1:T}} \frac{1}{T} \sum_{t=1}^T \sum_{i=1}^M \alpha_i I(\mathbf{x}_t; \boldsymbol{\eta}_{i,t}^G | \boldsymbol{\eta}_{1:t-1}^G) \quad (37a)$$

$$\text{s.t.} \quad \frac{1}{T} \sum_{t=1}^T \mathbb{E} \|\mathbf{x}_t - \hat{\mathbf{x}}_{t|t}\|^2 \leq \beta. \quad (37b)$$

We used Lemma 3 to write  $R_i^a$  in terms of the mutual informations  $I(\mathbf{x}_t; \boldsymbol{\eta}_{i,t}^G | \boldsymbol{\eta}_{1:t-1}^G)$ . Say  $\{V_t^*\}_{t=1}^T$  is a feasible solution of (37) and  $f^*$  is the attained value. Choosing the quantization sensitivities such that  $\frac{\Delta_{i,t}^2}{12} = V_{i,t}^*$  guarantees a (not-approximate) communication cost satisfying

$$\sum_{i=1}^M \alpha_i R_i \leq f^* + (1 + \frac{1}{2} \log \frac{2\pi e}{12}) \times \sum_{i=1}^M \alpha_i. \quad (38)$$

We also consider the infinite horizon problem where the quantizer sensitivities are time invariant, namely

$$\min_{\substack{V \in \mathbb{D}_+^M \\ t \in 1:T}} \limsup_{T \rightarrow \infty} \frac{1}{T} \sum_{t=1}^T \sum_{i=1}^M \alpha_i I(\mathbf{x}_t; \boldsymbol{\eta}_{i,t}^G | \boldsymbol{\eta}_{1:t-1}^G) \quad (39a)$$

$$\text{s.t.} \quad \limsup_{T \rightarrow \infty} \frac{1}{T} \sum_{t=1}^T \mathbb{E} \|\mathbf{x}_t - \hat{\mathbf{x}}_{t|t}\|^2 \leq \beta. \quad (39b)$$

In the following subsection, we describe an application of the sensor rate allocation optimization to resource management in remote sensing scenario.

#### F. Application example: physical layer resource allocation

The minimizations in (37) and (39) can be applied to a variety of resource allocation problems in wireless (and, in principle, wireline) communication systems. As an example, we consider a setup similar to the one proposed in [24], where several remote sensing platforms communicate their observations to a data fusion center a shared wireless medium. We present a simple example to conclude this section.

Consider the case where several remote sensors, using a fixed transmit power  $P_{TX}$  (in Watts), communicate their measurements to the fusion center via time-division multiple access (TDMA) over a channel of passband bandwidth  $B$  (in Hz). In such a system, the platforms take turns transmitting their measurements over the same bandlimited channel— see Figure 5. We assume that the  $i^{\text{th}}$  sensor platform is at range

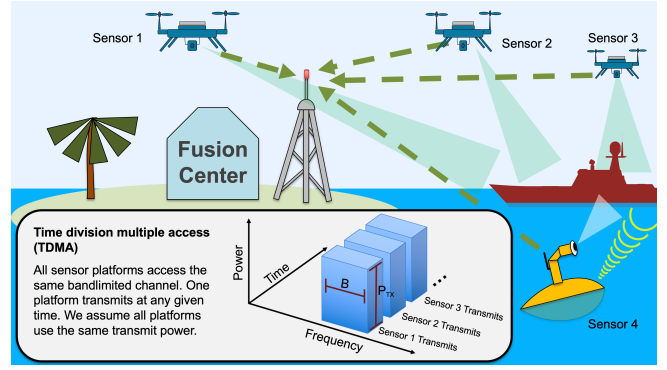


Fig. 5. In this example, the different sensor platforms relay their measurements to the fusion center over a common wireless link using TDMA (see inset).

of  $r_i$  from the fusion center, that all sensor platforms have identical transmission systems, and that the channel is line-of-sight. The amount of power received from transmitter  $i$  depends on range, as well as a variety of factors, like the gains from the antenna systems and the losses from other components. We let  $L$  encapsulate the factors that do not depend on range— in the present case  $L$  is assumed the same for all transmitters. The additive noise at the receiver is assumed to be white and Gaussian with power spectral density  $N_0$ . Since only one sensor platform transmits at any given time, the effective channel between the  $i^{\text{th}}$  transmitter and the fusion center is a point-to-point additive white Gaussian noise (AWGN) channel with a signal-to-noise ratio (SNR) of

$$\text{SNR}_i = L \frac{P_{TX}}{r_i^2 B N_0}. \quad (40)$$

The *capacity* of the wireless channel from receiver  $i$  to the fusion center is

$$C_i = B \log_2(1 + \text{SNR}_i) \text{ bits/second}, \quad (41)$$

which is the maximum reliable (e.g. error-free) data-rate that can be sustained from the  $i^{\text{th}}$  transmitter to the receiver. The *airtime*,  $\tau_i$ , in seconds, required to send  $b_i$  bits from the  $i^{\text{th}}$  sensor platform to the fusion center is lower bounded via

$$\tau_i \geq \frac{b_i}{C_i}. \quad (42)$$

This bound is in general loose, as the zero-error channel capacity is achievable only asymptotically (c.f. [30]). However, with modern error correcting codes (including low-density parity-check and turbo codes) is possible to communicate with very small error probability near the capacity for the point-to-point AWGN channel [31]. We thus make the assumption that

$$\tau_i \approx \frac{b_i}{C_i}. \quad (43)$$

In particular, the airtime is directly proportional to the energy expended on communication. Under the assumption that all the sensor platforms use the same transmit power, the energy expended to transmit  $b_i$  bits is  $E_i = P_{TX} \tau_i$ .

Minimizing the total airtime of a sensing task has a great deal of utility. It minimizes the amount of energy the network spends on communication. Furthermore, completing a sensing task with the minimum airtime is useful in and of itself, as may allow other users and systems the opportunity to access the channel without causing (or experiencing) additional interference. If we make the choice

$$\alpha_i = \frac{1}{C_i}, \quad (44)$$

the optimizations in (37) can be seen as minimizing the expected airtime (and, consequently, the energy expended on communication) required to complete the sensing task in the finite horizon. Note that the expected airtime expended by each sensor can vary over sampling periods, since at sampling period  $t$  sensor  $i$  will send an average of about  $\lceil I(\mathbf{x}_t; \boldsymbol{\eta}_{i,t}^G | \boldsymbol{\eta}_{1:t-1}^G) + 1.254 \rceil$  bits, where the mutual information is computed under the probability measure imposed by the minimizing policy.

It should be noted that, due our use of variable length coding, the required airtime is a random variable. In delay-tolerant applications, this may not be much of a problem. However, assume the sample rate of the sensors is fixed at  $T_s$ . The network will become congested if, during any sampling period, the required airtime exceeds  $T_s$ . In this setting, new measurements are being produced at a rate faster than the communication delay—more complicated scheduling algorithms may be required to ensure that the fusion center estimator achieves the desired performance by any real-time deadline (see, for example, [24]). If the expected airtime, per sampling period, obtained from the optimization (37) is small compared to  $T_s$ , the Markov inequality can be used to derive a simple bound on the congestion probability. These ideas can be extended to more general types of communication channels (e.g. fading channels) and corresponding more general notions of capacity.

### III. CONVERSION TO DIFFERENCE-OF-CONVEX PROBLEM

In this section, we reformulate (37) and (39) as difference of convex (DC) optimization problems. As defined earlier,  $P_{t|t-1}$  denotes the estimation error covariance of  $\mathbf{x}_t$  given  $\boldsymbol{\eta}_{1:t-1}^G$ . Similarly, we define  $P_{t|t-1}^{(i)}$  the error covariance of  $\mathbf{x}_t$  given  $\boldsymbol{\eta}_{1:t-1}^G$  and  $\boldsymbol{\eta}_{i,t}^G$ . Then, we have

$$P_{t|t-1}^{(i)} = (P_{t|t-1}^{-1} + C_i^\top V_{i,t}^{-1} C_i)^{-1}.$$

#### A. Reformulation of Mutual information

The mutual information (37a) can be expressed as:

$$I(\mathbf{x}_t; \boldsymbol{\eta}_{i,t}^G | \boldsymbol{\eta}_{1:t-1}^G) = h(\mathbf{x}_t | \boldsymbol{\eta}_{1:t-1}^G) - h(\mathbf{x}_t | \boldsymbol{\eta}_{1:t-1}^G, \boldsymbol{\eta}_{i,t}^G) \quad (45)$$

$$= \frac{1}{2} \log \det P_{t|t-1} - \frac{1}{2} \log \det P_{t|t-1}^{(i)} \quad (46)$$

$$= \frac{1}{2} \log \det P_{t|t-1} + \frac{1}{2} \log \det (P_{t|t-1}^{-1} + C_i^\top V_{i,t}^{-1} C_i) \quad (47)$$

$$= \frac{1}{2} \log \det (I + P_{t|t-1}^{\frac{1}{2}} C_i^\top V_{i,t}^{-1} C_i P_{t|t-1}^{\frac{1}{2}}) \quad (48)$$

$$= \frac{1}{2} \log (1 + V_{i,t}^{-\frac{1}{2}} C_i P_{t|t-1} C_i^\top V_{i,t}^{-\frac{1}{2}}) \quad (49)$$

$$= \frac{1}{2} \log V_{i,t}^{-1} + \frac{1}{2} \log (V_{i,t} + C_i P_{t|t-1} C_i^\top). \quad (50)$$

Introducing the new variables  $Q_{t|t-1} := P_{t|t-1}^{-1}$ ,  $Q_{t|t} := P_{t|t}^{-1}$  and  $\delta_{i,t} := V_{i,t}^{-1}$ , we can rewrite  $I(\mathbf{x}_t; \boldsymbol{\eta}_{i,t}^G | \boldsymbol{\eta}_{1:t-1}^G)$  as

$$\begin{aligned} I(\mathbf{x}_t; \boldsymbol{\eta}_{i,t}^G | \boldsymbol{\eta}_{1:t-1}^G) &= \frac{1}{2} \log \delta_{i,t} - \frac{1}{2} \log (\delta_{i,t}^{-1} + C_i Q_{t|t-1}^{-1} C_i^\top)^{-1} \\ &= \begin{cases} \min_{\gamma_{i,t}} & \frac{1}{2} \log \delta_{i,t} - \frac{1}{2} \log \gamma_{i,t} \\ \text{s.t.} & \gamma_{i,t} \leq (\delta_{i,t}^{-1} + C_i Q_{t|t-1}^{-1} C_i^\top)^{-1} \end{cases} \quad (51) \\ &= \begin{cases} \min_{\gamma_{i,t}} & \frac{1}{2} \log \delta_{i,t} - \frac{1}{2} \log \gamma_{i,t} \\ \text{s.t.} & \begin{bmatrix} \delta_{i,t} - \gamma_{i,t} & \delta_{i,t} C_i \\ C_i^\top \delta_{i,t} & Q_{t|t-1} + C_i^\top \delta_{i,t} C_i \end{bmatrix} \succeq 0. \end{cases} \quad (52) \end{aligned}$$

The slack variables  $\gamma_{i,t}$  were introduced in (51). To show (52), the matrix inversion lemma and Schur complement lemma are applied to the inequality constraint in (51).

#### B. Reformulation of mean square error

Using the variable  $Q_{t|t}$ , the fusion center's estimator MSE (37b) can be written as

$$\begin{aligned} \mathbb{E} \|\mathbf{x}_t - \hat{\mathbf{x}}_{t|t}^G\|^2 &= \text{Tr}(P_{t|t}) \\ &= \text{Tr}(Q_{t|t}^{-1}) \\ &= \begin{cases} \min_{S_t} & \text{Tr}(S_t) \\ \text{s.t.} & Q_{t|t}^{-1} \preceq S_t \end{cases} \\ &= \begin{cases} \min_{S_t} & \text{Tr}(S_t) \\ \text{s.t.} & \begin{bmatrix} S_t & I \\ I & Q_{t|t} \end{bmatrix} \succeq 0. \end{cases} \quad (54) \end{aligned}$$

The final step (54) follows from the Schur complement formula.

#### C. Reformulation of original problem (37)

Using (31), (52), and (54), problem (37) can be reformulated as:

$$\min \quad \frac{1}{T} \sum_{t=1}^T \sum_{i=1}^M \frac{\alpha_i}{2} (\log \delta_{i,t} - \log \gamma_{i,t}) \quad (55a)$$

$$\text{s.t.} \quad \begin{bmatrix} \delta_{i,t} - \gamma_{i,t} & \delta_{i,t} C_i \\ C_i^\top \delta_{i,t} & Q_{t|t-1} + C_i^\top \delta_{i,t} C_i \end{bmatrix} \succeq 0, \quad (55b)$$

$$\begin{bmatrix} S_t & I \\ I & Q_{t|t} \end{bmatrix} \succeq 0, \quad \frac{1}{T} \sum_{t=1}^T \text{Tr}(S_t) \leq \beta, \quad (55c)$$

$$Q_{t|t} = Q_{t|t-1} + \sum_{i=1}^M \delta_{i,t} C_i^\top C_i, \quad (55d)$$

$$Q_{t|t-1}^{-1} = A Q_{t-1|t-1}^{-1} A^\top + F F^\top, \quad (55e)$$

where the decision variables are  $[\delta_{i,t}, \gamma_{i,t}]$ , for  $i = 1, \dots, M$  and  $t = 1, \dots, T$ ,  $S_t$  for  $t = 1, \dots, T$ , and  $[Q_{t|t}, Q_{t|t-1}]$  for  $t = 2, \dots, T$ . The constraints (55d) and (55e) are imposed for  $t = 2, \dots, T$ , starting from  $Q_{1|1} = P_{1|1}^{-1}$ . All constraints in problem (55) are convex except (55e). In the following proposition, we show the non-convex constraint (55e) can be replaced by a convex constraint without changing the nature of the problem. More precisely, we show that the equality in (55e) can be replaced by an inequality and we can solve (56), instead of (55), to obtain the optimal rate allocation.

$$\min \quad \frac{1}{T} \sum_{t=1}^T \sum_{i=1}^M \frac{\alpha_i}{2} (\log \delta_{i,t} - \log \gamma_{i,t}) \quad (56a)$$

$$\text{s.t.} \quad \begin{bmatrix} \delta_{i,t} - \gamma_{i,t} & \delta_{i,t} C_i \\ C_i^\top \delta_{i,t} & Q_{t|t-1} + C_i^\top \delta_{i,t} C_i \end{bmatrix} \succeq 0, \quad (56b)$$

$$\begin{bmatrix} S_t & I \\ I & Q_{t|t} \end{bmatrix} \succeq 0, \quad \frac{1}{T} \sum_{t=1}^T \text{Tr}(S_t) \leq \beta, \quad (56c)$$

$$Q_{t|t} = Q_{t|t-1} + \sum_{i=1}^M \delta_{i,t} C_i^\top C_i, \quad (56d)$$

$$Q_{t|t-1}^{-1} \succeq A Q_{t-1|t-1}^{-1} A^\top + F F^\top \quad (56e)$$

**Proposition 1:** Let  $[\delta_{i,t}^*, \gamma_{i,t}^*, S_t^*, Q_{t|t}^*, Q_{t|t-1}^*]$  be the optimal solution for (56). Then,  $[\delta_{i,t}^*, \gamma_{i,t}^*, S_t^*, Q_{t|t}^{**}, Q_{t|t-1}^{**}]$  is the optimal solution for (55), where  $Q_{t|t}^{**}$  and  $Q_{t|t-1}^{**}$  are calculated recursively by

$$Q_{t|t-1}^{**} = A Q_{t-1|t-1}^{**} A^\top + F F^\top, \quad (57a)$$

$$Q_{t|t}^{**} = Q_{t|t-1}^{**} + \sum_{i=1}^M \delta_{i,t}^* C_i^\top C_i, \quad (57b)$$

starting from  $Q_{1|1}^{**} = Q_{1|1}^*$ . Moreover, if we denote the optimal values of (55) and (56) by  $J_1^*$  and  $J_2^*$  respectively, we have  $J_1^* = J_2^*$ .

*Proof:* As the first step of the proof, we show by induction that for  $t = 1, \dots, T$ , we have

$$Q_{t|t}^{**} \succeq Q_{t|t}^* \quad (58a)$$

$$Q_{t+1|t}^{**} \succeq Q_{t+1|t}^* \quad (58b)$$

For the initial step, (58a) trivially holds as  $Q_{1|1}^{**} = Q_{1|1}^*$  by construction. Note that  $Q_{2|1}^{**} = A Q_{1|1}^{**} A^\top + F F^\top$  by construction, and  $Q_{2|1}^{*-1} \succeq A Q_{1|1}^{*-1} A^\top + F F^\top$  since  $Q_{1|1}^*$  and  $Q_{2|1}^*$  are feasible solution to (55e). Thus  $Q_{2|1}^{**} \preceq Q_{2|1}^{*-1}$  or equivalently  $Q_{2|1}^{**} \succeq Q_{2|1}^*$ . Therefore, relation (58) holds for  $t = 1$ . For the induction step, we assume (58) holds for  $t = k (\geq 1)$ :

$$Q_{k|k}^{**} \succeq Q_{k|k}^*, \quad (59a)$$

$$Q_{k+1|k}^{**} \succeq Q_{k+1|k}^*, \quad (59b)$$

and we show that (58) holds for  $t = k + 1$ . From (55d) and (56d), we have

$$Q_{k+1|k+1}^{**} = Q_{k+1|k}^{**} + \sum_{i=1}^M \delta_{i,k+1}^* C_i^\top C_i \text{ and}$$

$$Q_{k+1|k+1}^* = Q_{k+1|k}^* + \sum_{i=1}^M \delta_{i,k+1}^* C_i^\top C_i$$

Thus, (59b) directly implies

$$Q_{k+1|k+1}^{**} \succeq Q_{k+1|k+1}^*. \quad (60)$$

Substituting  $Q_{k+1|k+1}^{**}$  into (55d), we have

$$Q_{k+2|k+1}^{**} = A Q_{k+1|k+1}^{**} A^\top + F F^\top \quad (61a)$$

$$\succeq A Q_{k+1|k+1}^{*-1} A^\top + F F^\top \quad (61b)$$

$$\succeq Q_{k+2|k+1}^{*-1}, \quad (61c)$$

where (61b) is due to (60). The last inequality holds since  $(Q_{k+1|k+1}^*, Q_{k+2|k+1}^*)$  is a feasible solution satisfying (56d). (61) implies

$$Q_{k+2|k+1}^{**} \succeq Q_{k+2|k+1}^*. \quad (62)$$

Inequalities (60) and (62) establish the relation (58) for  $t = k + 1$  and thus for any  $t = 1 : T$ . This completes the first step of the proof.

The proof can be completed as follows. Let  $J_2^*$  be the optimal value of (56) attained by  $[\delta_{i,t}^*, \gamma_{i,t}^*, S_t^*, Q_{t|t}^*, Q_{t|t-1}^*]$ . From (58), we have

$$\begin{aligned} 0 &\preceq \begin{bmatrix} \delta_{i,t}^* - \gamma_{i,t}^* & \delta_{i,t}^* C_i \\ C_i^\top \delta_{i,t}^* & Q_{t|t-1}^* + C_i^\top \delta_{i,t}^* C_i \end{bmatrix} \\ &\preceq \begin{bmatrix} \delta_{i,t}^* - \gamma_{i,t}^* & \delta_{i,t}^* C_i \\ C_i^\top \delta_{i,t}^* & Q_{t|t-1}^{**} + C_i^\top \delta_{i,t}^* C_i \end{bmatrix} \\ 0 &\preceq \begin{bmatrix} S_t^* & I \\ I & Q_{t|t}^* \end{bmatrix} \preceq \begin{bmatrix} S_t^* & I \\ I & Q_{t|t}^{**} \end{bmatrix}. \end{aligned}$$

Moreover,  $(Q_{t|t}^{**}, Q_{t|t-1}^{**})$  satisfies the equality constraints (57) by construction. This means that  $[\delta_{i,t}^*, \gamma_{i,t}^*, S_t^*, Q_{t|t}^{**}, Q_{t|t-1}^{**}]$  is a feasible solution of equation (55) and it obtains the value  $J_2^*$ . Therefore,  $J_1^* \leq J_2^*$ . However, (55) has more strict constraint than (56) which immediately implies  $J_1^* \geq J_2^*$ . Therefore,  $J_1^* = J_2^*$ . ■

Constraint (56e) can be written as an equivalent linear matrix inequality (LMI) [32] condition. Therefore, problem (37) can be written as:

$$\min \quad \frac{1}{T} \sum_{t=1}^T \sum_{i=1}^M \frac{\alpha_i}{2} (\log \delta_{i,t} - \log \gamma_{i,t}) \quad (64a)$$

$$\text{s.t.} \quad \begin{bmatrix} \delta_{i,t} - \gamma_{i,t} & \delta_{i,t} C_i \\ C_i^\top \delta_{i,t} & Q_{t|t-1} + C_i^\top \delta_{i,t} C_i \end{bmatrix} \succeq 0, \quad (64b)$$

$$\begin{bmatrix} S_t & I \\ I & Q_{t|t} \end{bmatrix} \succeq 0, \quad \frac{1}{T} \sum_{t=1}^T \text{Tr}(S_t) \leq \beta, \quad (64c)$$

$$Q_{t|t} = Q_{t|t-1} + \sum_{i=1}^M \delta_{i,t} C_i^\top C_i. \quad (64d)$$

$$\begin{bmatrix} Q_{t|t-1} & Q_{t|t-1} A & Q_{t|t-1} F \\ A^\top Q_{t|t-1} & Q_{t-1|t-1} & 0 \\ F^\top Q_{t|t-1} & 0 & I \end{bmatrix} \succeq 0. \quad (64e)$$

It is simple to verify that (64) is the minimization of the difference of two convex functions subject to convex constraints and thus it is an instance of a difference-of-convex

program. The infinite horizon (time-invariant) counterpart of (64) can be formulated as:

$$\min \sum_{i=1}^M \frac{\alpha_i}{2} (\log \delta_i - \log \gamma_i) \quad (65a)$$

$$\text{s.t.} \quad \begin{bmatrix} \delta_i - \gamma_i & \delta_i C_i \\ C_i^\top \delta_i & \hat{Q} + C_i^\top \delta_i C_i \end{bmatrix} \succeq 0, \forall i = 1, \dots, M, \quad (65b)$$

$$Q = \hat{Q} + \sum_{i=1}^M \delta_i C_i^\top C_i, \quad \text{Tr}(S) \leq \beta, \quad (65c)$$

$$\begin{bmatrix} S & I \\ I & Q \end{bmatrix} \succeq 0, \quad \begin{bmatrix} \hat{Q} & \hat{Q}A & \hat{Q}F \\ A^\top \hat{Q} & Q & 0 \\ F^\top \hat{Q} & 0 & I \end{bmatrix} \succeq 0. \quad (65d)$$

#### IV. CONVEX-CONCAVE PROCEDURE (CCP)

In this section, we develop an iterative algorithm based on the convex-concave procedure (CCP) [5] to find local minimums of the time-varying and time-invariant sensor data-rate allocation problems (64) and (65). CCP starts by over-approximating the non-convex terms of the DC program via linearization around a nominal point. The resulting convex problem can then be solved efficiently, and the algorithm iterates by convexifying the problem around the obtained solution. The process terminates when a local minimum is found. Starting from a feasible nominal point, as it is shown in [5], all subsequent iterations will be feasible and the algorithm converges to a local minima.

We now show how the CCP algorithm operates for the time-invariant problem (65). For this problem, we linearize the non-convex term  $\log \delta_i$  around the nominal point  $\hat{\delta}_i$  which gives an upper bound to  $\log \delta_i$  as  $\log \delta_i \leq \frac{1}{\hat{\delta}_i}(\delta_i - \hat{\delta}_i) + \log \hat{\delta}_i$ . Thus, at each iteration of CCP algorithm we solve:

$$\min \sum_{i=1}^M \frac{\alpha_i}{2} (\delta_i / \hat{\delta}_i - 1 + \log \hat{\delta}_i - \log \gamma_i) \quad (66a)$$

$$\text{s.t.} \quad (65b) - (65d). \quad (66b)$$

If we denote the solution of (66) at iteration  $k$  by  $(\delta_i^k, \gamma_i^k, S^k, Q^k, \hat{Q}^k)$ , at iteration  $k+1$  (66) is solved for  $\hat{\delta}_i = \delta_i^k$ . Note that the optimal value of (66) is an upper bound for the optimal value of (65) with same decision variables  $S, Q, \hat{Q}, \delta_i$ , and  $\gamma_i$  for  $i = 1, \dots, M$ . The CCP algorithm we use to perform the time-invariant optimization (65) is outlined in Algorithm 1. A similar algorithm can be used to solve (64).

---

#### Algorithm 1: Convex-Concave Procedure (CCP)

---

Set *tolerance* sufficiently small; Set initial value  $\hat{\delta}_i \leftarrow 1$  for  $i = 1, 2, \dots, M$ ;  
**for**  $k = 1, 2, \dots$  **do**  
    Solve (66);  
     $(\delta_i^k, \gamma_i^k, S^k, Q^k, \hat{Q}^k) \leftarrow$  Obtain optimal solution;  
    Update  $\hat{\delta}_i \leftarrow \delta_i^k$  for  $i = 1 : M$ ;  
    Break if  $f^{k-1} - f^k \leq \text{tolerance}$ ;

---

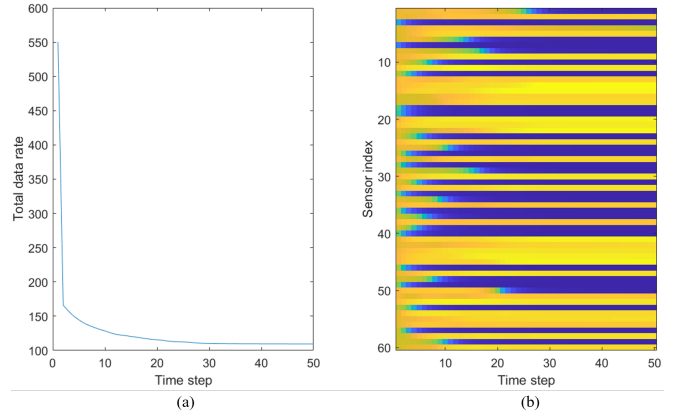


Fig. 6. CCP data rate ( $\beta = 0.1$ ). (a) Total data rate (b) sensor data rate allocation.

#### V. NUMERICAL ANALYSIS

In this section, we present two numerical simulations showing the effectiveness of Algorithm 1. In both studies, we assign  $\alpha_i = 1$  for all sensors.

##### A. Heat diffusion system

We first consider the problem of estimating the temperature distribution over a time-invariant 1D heat diffusion system [33]. We assume a 15m thin concrete rod and the spatial domain is equally divided by 60 nodes. The heat transfer model is given by (1) with

$$A = \frac{a}{h^2} \begin{bmatrix} 2 & -1 & & & \\ & -1 & 2 & -1 & \\ & & \ddots & \ddots & \ddots \\ & & & -1 & 2 & -1 \\ & & & & -1 & 2 \end{bmatrix}$$

where  $a = 7.5 \times 10^{-7}$  is thermal diffusivity and  $h = 0.2459$  is the length of each segment. We also assume there is a random heat input to each node; this is modeled as (1) with  $F = I$ .

Suppose that a sensor is placed at each node, measuring the node's temperature noiselessly. The measurement data is transmitted to a data fusion center over a communication network. Fig. 6 shows the performance of Algorithm 1 when the communication cost is  $\beta = 0.1$ . The algorithm is initialized with the data rate equally allocated to each sensor. However, as the iteration proceeds, the allocated data rate is updated as presented in Fig 6 (b) and the total data rate converges as shown in Fig 6 (a).

Fig. 7 shows the data rate allocation obtained after a sufficient number of CCP iterations with three different values of  $\beta$ . We observe that similar subset of sensors are given non-zero data rate with these  $\beta$  values. However, allocated data rates to individual sensors decrease as  $\beta$  increases. Moreover, more sensors are allocated zero data rate as  $\beta$  increases.

To confirm the last observation, Fig. 8 presents the number of sensors allocated non-zero data rate after a sufficient number of CCP iterations when  $\beta$  is varied from 1 to 220.

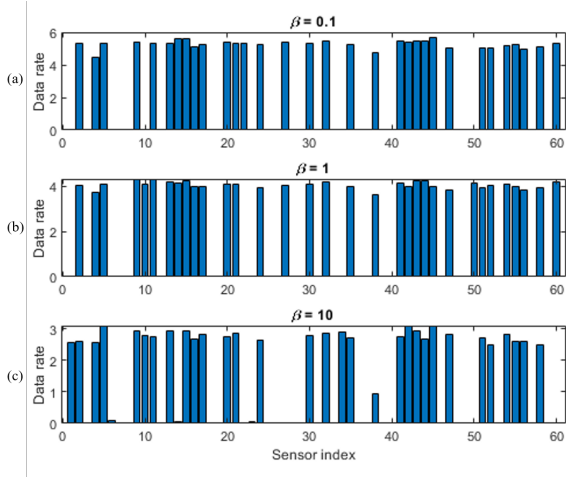


Fig. 7. Data rate allocation obtained by CCP with (a)  $\beta = 0.1$  (b)  $\beta = 1$  (c)  $\beta = 10$ .

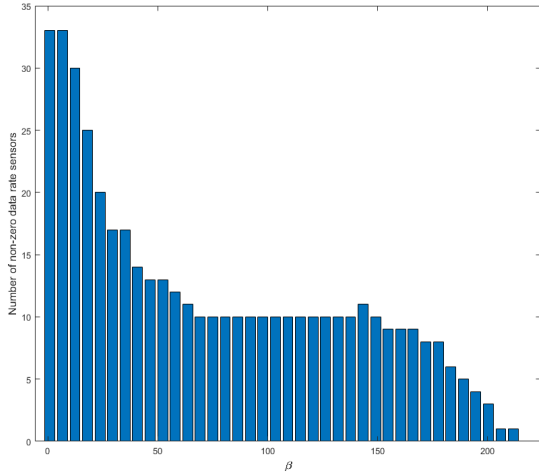


Fig. 8. Number of sensors allocated non-zero data rate by CCP tested over the range  $1 \leq \beta \leq 220$ .

The number of sensors tends to decrease, but is somewhat stagnant in the middle of the beta range. The relationship is not necessarily monotone. This plot shows a sparsity-promoting property of the proposed data rate allocation method.

### B. Target tracking by a drone swarm

Next, we consider the problem tracking multiple moving targets using a radar signal and multiple drones. As in [34], we consider a scenario in which a base station, which also serves as the data fusion center, illuminates the targets with a radar signal, and the drones make time-delay and Doppler measurements of the reflected signal from the targets. Drones transmit these measurements back to the data fusion center, where the targets' positions are estimated by an Extended Kalman Filter (EKF). Unlike the previous example, the system "C" matrix in (2) is time-varying as relative positions of the drones with respect to the targets change over time. Therefore, we consider an approach to recalculate the rate

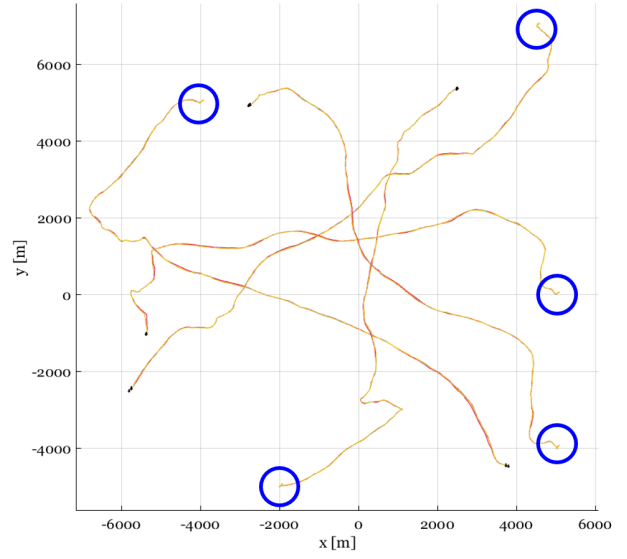


Fig. 9. Target tracking simulation result in 5 separate regions.

allocation at every time step by a repetitive execution of Algorithm 1. To improve computational efficiency, we adopt a "warm start" implementation of Algorithm 1 at every time step, i.e., the optimal allocation from the previous time step is used as the initial condition for the CCP iteration in the next time step.

We assume there are five targets in the entire 2D environment. Each target is assumed to be a point mass driven by a random force which is modeled as an i.i.d. Gaussian process noise. The state vector to be estimated in this simulation study is therefore (1) with

$$x_t = [x_t^1 \ x_t^2 \ x_t^3 \ x_t^4 \ x_t^5]^\top \in \mathbb{R}^{20}$$

where  $x_t^i = [p_{x,t}^i \ p_{y,t}^i \ v_{x,t}^i \ v_{y,t}^i]^\top$  are the position and the velocity of the  $i$ -th target, and  $A = \text{diag}(A_{\text{Target}}, A_{\text{Target}}, A_{\text{Target}}, A_{\text{Target}}, A_{\text{Target}})$  with

$$A_{\text{Target}} = \begin{bmatrix} 1 & 0 & \Delta_t & 0 \\ 0 & 1 & 0 & \Delta_t \\ 0 & 0 & 1 & 0 \\ 0 & 0 & 0 & 1 \end{bmatrix}.$$

where  $\Delta_t = 1$  is the step size. We assume  $FF^\top = \text{diag}(10, 10, 1, 1)$ .

As shown in Fig. 9, we assume that five drones are available in the neighborhood of each target (so there are 25 drones in total). Each drone is modeled as a point mass in a 2D plane. Let  $(p_{x,t}^{i,j}, p_{y,t}^{i,j})$  be the coordinate of the  $j$ -th drone in the neighborhood of the  $i$ -th target, and  $(v_{x,t}^{i,j}, v_{y,t}^{i,j})$  be its velocity. Drones are controlled by the data fusion center to track the target. In this simulation, we assume that a PD control with acceleration input is used for each drone:

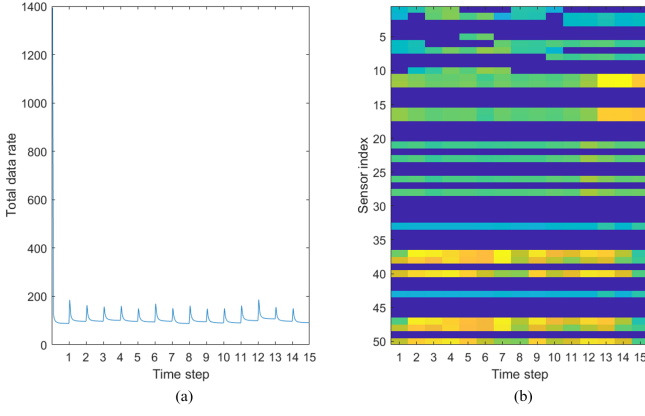


Fig. 10. CCP data rate for 15 time steps ( $\beta = 1$ ). (a) Total data rate (b) Sensor data rate allocation.

$$\begin{aligned}
 a_{x,t}^{i,j} &= K_P(\hat{p}_{x,t}^i - p_{x,t}^{i,j}) + K_D(\hat{v}_{x,t}^i - v_{x,t}^{i,j}) \\
 &\quad - \sum_{k \neq j} L_P(p_{x,t}^{i,k} - p_{x,t}^{i,j}) - \sum_{k \neq j} L_D(v_{x,t}^{i,k} - v_{x,t}^{i,j}) \\
 a_{y,t}^{i,j} &= K_P(\hat{p}_{y,t}^i - p_{y,t}^{i,j}) + K_D(\hat{v}_{y,t}^i - v_{y,t}^{i,j}) \\
 &\quad - \sum_{k \neq j} L_P(p_{y,t}^{i,k} - p_{y,t}^{i,j}) - \sum_{k \neq j} L_D(v_{y,t}^{i,k} - v_{y,t}^{i,j}).
 \end{aligned} \tag{67}$$

Here,  $(\hat{p}_{x,t}^i, \hat{p}_{y,t}^i, \hat{v}_{x,t}^i, \hat{v}_{y,t}^i)$  is the estimated state of the target  $i$  computed by the data fusion center using the EKF described below. The gains  $K_P$  and  $K_D$  are tuned to keep the drones close to the target, whereas gains  $L_P$  and  $L_D$  are selected so that drones in the same neighborhood stay away from each other.

At every time step, the base station illuminates the targets with a radar signal. We assume that the reflected signal from the  $i$ -th target is observed by the drones in the  $i$ -th region. The  $j$ -th drone in the  $i$ -th region obtains the Doppler estimate  $f_t^{i,j}$  and the time delay  $\tau_t^{i,j}$  of the signal, which are given as follows [34]:

$$\begin{aligned}
 f_t^{i,j} &= \frac{(v_{x,t}^i p_{x,t}^{i,j} + v_{y,t}^i p_{y,t}^{i,j})}{\sqrt{(p_{x,t}^i)^2 + (p_{y,t}^i)^2}} \\
 &\quad + \frac{(v_{x,t}^i - v_{x,t}^{i,j})(p_{x,t}^i - p_{x,t}^{i,j}) + (v_{y,t}^i - v_{y,t}^{i,j})(p_{y,t}^i - p_{y,t}^{i,j})}{\sqrt{(p_{x,t}^i - p_{x,t}^{i,j})^2 + (p_{y,t}^i - p_{y,t}^{i,j})^2}}
 \end{aligned} \tag{68}$$

$$\tau_t^{i,j} = \sqrt{(p_{x,t}^i)^2 + (p_{y,t}^i)^2} + \sqrt{(p_{x,t}^i - p_{x,t}^{i,j})^2 + (p_{y,t}^i - p_{y,t}^{i,j})^2} \tag{69}$$

Since (68) and (69) are nonlinear observations of the state vector  $x_t$ , we linearize them around the current best estimate  $(\hat{p}_{x,t}^i, \hat{p}_{y,t}^i, \hat{v}_{x,t}^i, \hat{v}_{y,t}^i)$ , where these estimates are recursively computed using the EKF.

Fig. 9 shows the scenario described above simulated for 1,000 time steps. Blue circles represent neighborhood regions of each target, and there are five drones in each region. The target trajectory is presented as red line and drone trajectories

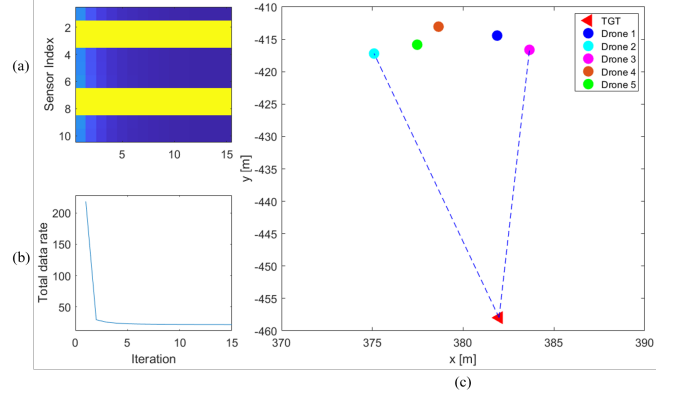


Fig. 11. Data rate allocation in Region 1 at  $t=70$  ( $\beta = 1$ ). (a) Sensor data rate allocation. Indices 1-5 correspond to the time delay measurements  $\tau_t^{1,j}, j = 1, \dots, 5$  and indices 6-10 correspond to the Doppler estimates  $f_t^{1,j}, j = 1, \dots, 5$ ; (b) total data rate; (c) position of target and drones.

in other colors. Based on the calculated position and velocity of target and drones, we apply the CCP iterations in each time step. Fig. 10 shows the rate allocation obtained after a sufficient number of CCP iterations in each step for the first 15 time steps. The result is changing over time, reflecting the time-varying nature of the considered problem. To gain further intuition on this simulation result, Fig 11 shows the data rate allocated to drones in region 1 and their spatial positions at time step  $t = 70$ . Fig 11 (a) indicates that non-zero data rates are given only to sensors 2,3,7 and 8, which corresponds to delay measurements and Doppler estimates from drones 2 and 3. Fig 11 (c) indicates that drones 2 and 3 are the left-most and the right-most vehicles in the formation.

## VI. DISCUSSION

As observed in Section V, the SRA formulation (39) (similarly, (37)) admits sparse solutions, in other words, for several sensors we have  $\delta_i = 0$ . In this section, we take a closer look at the mathematical structure of SRA problem. We first remark that the sparsity-promoting nature of the solution can be attributed, at least in part, to mathematical structure of the communication cost. The communication cost (56a) is reminiscent of the *sum-of-logs* regularizer, a widely used heuristic to induce sparse solutions [35].

To develop further insight, we consider a special case of sensor rate allocation problem for which the closed-form solution is available. Consider a scalar system described by

$$\mathbf{x}_{t+1} = a\mathbf{x}_t + f\mathbf{w}_t, \quad \mathbf{w}_t \stackrel{i.i.d.}{\sim} \mathcal{N}(0, 1),$$

and a single measurement

$$\eta_t = \mathbf{x}_t + \mathbf{v}_t, \quad \mathbf{v}_t \stackrel{i.i.d.}{\sim} \mathcal{N}(0, V_t).$$

Since the system is observable,  $P \triangleq \lim_{t \rightarrow \infty} P_{t|t}$  exists and is computed by the algebraic Riccati equation (ARE)

$$P^{-1} = (a^2 P + f^2)^{-1} + V^{-1}, \tag{71}$$

where  $V \triangleq \limsup_{t \rightarrow \infty} V_t$ . The time-invariant rate allocation problem (39) for this system is

$$\min_{P, V \geq 0} \log(a^2 + \frac{f^2}{P}) \quad (72a)$$

$$\text{s.t. } P \leq \beta \quad (72b)$$

$$P^{-1} = (a^2 P + f^2)^{-1} + V^{-1}. \quad (72c)$$

Denote by  $P = g(V)$  the unique positive solution to the ARE (71). It is easy to show that  $g(V)$  is a strictly increasing, and thus invertible, function of  $V$  with a bounded range  $[g(0) = 0, g(\infty) = \frac{f^2}{1-a^2}]$ . Therefore, the problem (72) can be equivalently written as

$$\min_{P \geq 0} \log(a^2 + \frac{f^2}{P}) \quad (73a)$$

$$\text{s.t. } P \leq \beta \quad (73b)$$

$$P \leq \frac{f^2}{1-a^2}. \quad (73c)$$

It is straightforward to verify that the minimizer of (73) is  $P^* = \min\{\beta, \frac{f^2}{1-a^2}\}$  and the optimal value of (73) is  $\min\{0, \log(a^2 + \frac{f^2}{\beta})\}$ . The  $P^*$  is obtained by adopting  $V^* = g^{-1}(P^*)$ . The condition  $P^* = \frac{f^2}{1-a^2}$ , leading to  $V^* = \infty$ , corresponds to the condition when it is optimal to allot zero data rate to the sensor. This partly explains the sparse nature of the solutions we observed in Section V. It is worth noting that problem (73) is equivalent to scalar infinite-horizon sequential rate-distortion problem studied in [36], [37].

## VII. CONCLUSION

In this paper, we considered a sensor data rate allocation problem for dynamic sensor fusion over resource restricted communication networks. Using a system model motivated by practical remote sensing scenarios and well-understood methods of zero delay source coding, we proposed a data rate allocation problem between a group of remote sensors and a fusion center. We reformulated this problem using information theoretic tools and ideas from Kalman filtering. Our proposed optimization took the form of a difference-of-convex program. We applied the CCP algorithm to find a heuristic solution. We conducted a numerical study on a 1D heat transfer model and on a 2D target tracking by drone swarm scenario. Our numerical results suggest that the proposed approach is sparsity-promoting. By considering a limiting case of the SRA problem that admitted an analytical solution, we gained insight into the sparsity promoting property. Possible directions for future research include analyzing the non-convexity of the SRA problem and developing computationally efficient algorithms to perform the minimization. In addition, a connection to the CEO problem and extensions to unreliable networks are attractive avenues for future research.

## REFERENCES

- [1] J. Collins, "The challenges facing u.s. navy aircraft electrical wiring systems," in *Proceedings of the 9th Annual Aging Aircraft Conference*. US Federal Aviation Administration, Department of Defence, and the National Aeronautics and Space Agency, 2006.
- [2] B. Marr, "That's data science: Airbus puts 10,000 sensors in every single wing," Online, 2015, <https://www.datasciencecentral.com/profiles/blogs/that-s-data-science-airbus-puts-10-000-sensors-in-every-single>.
- [3] R. Zamir and M. Feder, "On universal quantization by randomized uniform/lattice quantizers," *IEEE Transactions on Information Theory*, vol. 38, no. 2, pp. 428–436, 1992.
- [4] T. Tanaka, K. H. Johansson, T. Oechtering, H. Sandberg, and M. Skoglund, "Rate of prefix-free codes in LQG control systems," in *2016 IEEE International Symposium on Information Theory (ISIT)*. IEEE, 2016, pp. 2399–2403.
- [5] T. Lipp and S. Boyd, "Variations and extension of the convex-concave procedure," *Optimization and Engineering*, vol. 17, no. 2, pp. 263–287, 2016.
- [6] H. Jung and T. Tanaka, "Optimal data rate allocation for dynamic sensor fusion over resource constrained communication networks," in *Proc. of the 2021 American Control Conference (ACC)*. IEEE, 2021, to be published.
- [7] D. Kammer, "Sensor placement for on-orbit modal identification and correlation of large space structures," in *1990 American Control Conference*. IEEE, 1990, pp. 2984–2990.
- [8] L. Yao, W. Sethares, and D. Kammer, "Sensor placement for on-orbit modal identification of large space structure via a genetic algorithm," in *[Proceedings 1992] IEEE International Conference on Systems Engineering*. IEEE, 1992, pp. 332–335.
- [9] H. Wang, K. Yao, G. Pottie, and D. Estrin, "Entropy-based sensor selection heuristic for target localization," in *In Proceedings of the 3rd International Symposium on Information Processing in Sensor Networks*. Berkeley, CA, USA: IEEE, 2004, pp. 36–45.
- [10] S. Joshi and S. Boyd, "Sensor selection via convex optimization," *IEEE Transactions on Signal Processing*, vol. 57, no. 2, pp. 451–462, 2009.
- [11] G. M. Hoffmann and C. J. Tomlin, "Mobile sensor network control using mutual information methods and particle filters," *IEEE Transactions on Automatic Control*, vol. 55, no. 1, pp. 32–47, 2010.
- [12] Q. Yan and J. Chen, "Sensor selection via maximizing hybrid bayesian fisher information and mutual information in unreliable sensor networks," *Electronics*, vol. 9, no. 2, 2020. [Online]. Available: <https://www.mdpi.com/2079-9292/9/2/283>
- [13] Y. Mo, R. Ambrosino, and B. Sinopoli, "Sensor selection strategies for state estimation in energy constrained wireless sensor networks," *Automatica*, vol. 47, no. 7, pp. 1330–1338, 2011. [Online]. Available: <https://www.sciencedirect.com/science/article/pii/S0005109811001026>
- [14] L. Liu, D. Liu, Y. Zhang, and Y. Peng, "Effective sensor selection and data anomaly detection for condition monitoring of aircraft engines," *Sensors*, vol. 16, no. 5, 2016. [Online]. Available: <https://www.mdpi.com/1424-8220/16/5/623>
- [15] E. I. Silva, M. S. Derpich, and J. Ostergaard, "A framework for control system design subject to average data-rate constraints," *IEEE Trans. Automat. Cont.*, vol. 56, no. 8, pp. 1886–1899, 2011.
- [16] J. Stefan and T. Tanaka, "Sparse lqr synthesis via information regularization," in *2019 IEEE 58th Conference on Decision and Control (CDC)*. IEEE, 2019, pp. 7345–7351.
- [17] T. Berger, Z. Zhang, and H. Viswanathan, "The ceo problem [multi-terminal source coding]," *IEEE Transactions on Information Theory*, vol. 42, no. 3, pp. 887–902, 1996.
- [18] H. Viswanathan and T. Berger, "The quadratic gaussian ceo problem," *IEEE Transactions on Information Theory*, vol. 43, no. 5, pp. 1549–1559, 1997.
- [19] V. Kostina and B. Hassibi, "Fundamental limits of distributed tracking," *arXiv preprint, arXiv: 1910.02534*, 2020. [Online]. Available: <https://arxiv.org/abs/1910.02534>
- [20] J. Massey, "Causality, feedback and directed information," in *Proc. IEEE ISIT*. IEEE, 1990, pp. 303–305.
- [21] O. N. Yilmaz, Y.-P. E. Wang, N. A. Johansson, N. Brahm, S. A. Ashraf, and J. Sachs, "Analysis of ultra-reliable and low-latency 5G communication for a factory automation use case," in *2015 IEEE international conference on communication workshop (ICCW)*. IEEE, 2015, pp. 1190–1195.

- [22] G. Durisi, T. Koch, and P. Popovski, "Toward massive, ultrareliable, and low-latency wireless communication with short packets," *Proceedings of the IEEE*, vol. 104, no. 9, pp. 1711–1726, 2016.
- [23] Z. Hou, C. She, Y. Li, L. Zhuo, and B. Vucetic, "Prediction and communication co-design for ultra-reliable and low-latency communications," *IEEE Transactions on Wireless Communications*, vol. 19, no. 2, pp. 1196–1209, 2020.
- [24] R. Jurdi, J. G. Andrews, and R. W. Heath, "Scheduling observers over a shared channel with hard delivery deadlines," *IEEE Transactions on Communications*, vol. 69, no. 1, pp. 133–148, 2021.
- [25] D. Baumann, F. Mager, U. Wetzker, L. Thiele, M. Zimmerling, and S. Trimpe, "Wireless control for smart manufacturing: Recent approaches and open challenges," *Proceedings of the IEEE*, vol. 109, no. 4, pp. 441–467, 2021.
- [26] T. Cover and J. Thomas, *Elements of Information Theory*, 2nd ed. Wiley-Interscience, 2006.
- [27] S. Yüksel, "Jointly optimal LQG quantization and control policies for multi-dimensional systems," *IEEE Transactions on Automatic Control*, vol. 59, no. 6, pp. 1612–1617, 2014.
- [28] M. S. Derpich and J. Ostergaard, "Improved upper bounds to the causal quadratic rate-distortion function for gaussian stationary sources," *IEEE Transactions on Information Theory*, vol. 58, no. 5, pp. 3131–3152, 2012.
- [29] E. Silva, "A unified framework for the analysis and design of networked control systems," Ph.D. dissertation, School of Electric Engineering and Computer Science, University of Newcastle, Callaghan, Australia, 2009.
- [30] Y. Polyanskiy, H. V. Poor, and S. Verdú, "Channel coding rate in the finite blocklength regime," *IEEE Transactions on Information Theory*, vol. 56, no. 5, pp. 2307–2359, 2010.
- [31] D. J. Costello and G. D. Forney, "Channel coding: The road to channel capacity," *Proceedings of the IEEE*, vol. 95, no. 6, pp. 1150–1177, 2007.
- [32] S. Boyd, L. Ghaoui, E. Feron, and V. Balakrishnan, *Linear Matrix Inequalities in System and Control Theory*, 1st ed., ser. SIAM Studies in Applied Mathematics. SIAM, 1994, ch. 2, sec. 2-2, pp. 7–12. [Online]. Available: <https://web.stanford.edu/~boyd/lmibook/lmibook.pdf>
- [33] Y. Chahlaoui, "A collection of benchmark examples for model reduction of linear time invariant dynamical systems," Subroutine Library in Systems and Control Theory, Online, SLICOT Working Note 2002-2, Feb. 2002. [Online]. Available: <http://slicot.org/20-site/126-benchmark-examples-for-model-reduction>
- [34] P. Zhan, D. Casbeer, and A. Swindlehurst, "A centralized control algorithm for target tracking with UAVs," in *Conference Record of the Thirty-Ninth Asilomar Conference on Signals, Systems and Computers*, 2005. IEEE, 2005, pp. 1148–1152.
- [35] E. J. Candes, M. B. Wakin, and S. P. Boyd, "Enhancing sparsity by reweighted l1 minimization," *J. Fourier analysis and applications*, vol. 14, no. 5-6, pp. 877–905, 2008.
- [36] T. Tanaka, K.-K. K. Kim, P. A. Parrilo, and S. K. Mitter, "Semidefinite programming approach to gaussian sequential rate-distortion trade-offs," *IEEE Transactions on Automatic Control*, vol. 62, no. 4, pp. 1896–1910, 2016.
- [37] S. Tatikonda, A. Sahai, and S. Mitter, "Stochastic linear control over a communication channel," *IEEE transactions on Automatic Control*, vol. 49, no. 9, pp. 1549–1561, 2004.